Atmospheric Environment 294 (2023) 119436

Contents lists available at ScienceDirect

Atmospheric Environment

journal homepage: www.elsevier.com/locate/atmosenv

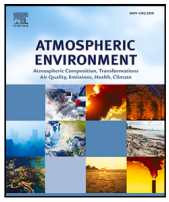

Continental-scale Atmospheric Impacts of the 2020 Western U.S. Wildfires

I.S. Albores [a,b], R.R. Buchholz [c,*], I. Ortega [c], L.K. Emmons [c], J.W. Hannigan [c], F. Lacey [c,d], G. Pfister [c], W. Tang [c], H.M. Worden [c]

[a] Williams College, Williamstown, MA, United States of America
[b] University Corporation for Atmospheric Research, Boulder, CO, United States of America
[c] Atmospheric Chemistry Observations & Modeling Laboratory, National Center for Atmospheric Research, Boulder, CO, United States of America
[d] Research Applications Laboratory, National Center for Atmospheric Research, Boulder, CO, United States of America

HIGHLIGHTS

- The 2020 Western U.S. wildfires produced CO emissions 3 times the 2001–2019 average.
- The fires contributed 0.5 – 14.5% to modeled CO averaged over the United States.
- Enhancements in surface O_3 and $PM_{2.5}$ across the U.S. lasted through the fire season.

ARTICLE INFO

Keywords:
Wildfire
Ozone
Carbon monoxide
CAM-chem

ABSTRACT

The wildfire season in the Western United States (U.S.) was anomalously large in 2020, with a majority of burned area due to lightning ignitions resulting in overall fire emissions of carbon monoxide (CO) in the Western region almost 3 times the 2001–2019 average. We used the Community Atmosphere Model version 6 with Chemistry (CAM-chem) to investigate how the 2020 fires in the Western U.S. affected air quality locally as well as in surrounding regions that received transported pollution. Simulations with and without fire emissions over the Western U.S. (32.5–49° N, 115–125° W) in July–December 2020 were used to determine average changes in atmospheric composition across the country. Comparisons against satellite and ground-based column CO observations show that the model generally underestimated CO from fires but adequately reproduced spatial and temporal variability. Simulations showed the 2020 fire season contributed 14.5% to atmospheric CO over the Contiguous United States in September, and ~3% to CO averaged across the Northern Hemisphere; these enhancements lasted several months. Fire emissions in 2020 continued later into the year than usual, resulting in sustained air pollution over the Western U.S. region, with noticeable meridional transport of ozone (O_3) and fine particulate matter ($PM_{2.5}$). Finally, we use the model to identify two transported fire pollution events at Boulder, Colorado.

1. Introduction

Fires in the Western region of the United States have been increasing in frequency (Dennison et al., 2014). Through the analysis of satellite mapping, Dennison et al. (2014) identified climate change as a significant factor in the positive trend in the number and size of forest fires in northwestern regions of the United States between 1984 and 2011. In the Pacific Northwest (PNW), it is estimated that anthropogenic climate change doubled the forest fire area (Abatzoglou and Williams, 2016). Similar increasing trends in forest fire numbers and size are likely to persist as anthropogenic climate change continues (Xu et al., 2020, e.g.).

Through emissions, fires impact atmospheric composition, contributing both long and short-lived trace gases and aerosols to the atmosphere (Voulgarakis and Field, 2015) that can detrimentally affect air quality. Air quality is vital to human health and quality of life, and the impact of fires on air quality is increasingly a concern (Finlay et al., 2012). Although there have been successful efforts to improve air quality throughout the United States in recent decades by reducing human-made pollution throughout the United States, the growing prevalence of wildfires has inhibited air quality improvement in fire-prone regions (McClure and Jaffe, 2018).

* Correspondence to: National Center for Atmospheric Research, Atmospheric Chemistry Observations & Modeling Laboratory, Boulder, CO 80301, United States of America.
E-mail address: buchholz@ucar.edu (R.R. Buchholz).

https://doi.org/10.1016/j.atmosenv.2022.119436
Received 20 March 2022; Received in revised form 30 September 2022; Accepted 20 October 2022
Available online 5 November 2022

The emissions created by wildfires can influence atmospheric chemical species in areas far from the fire sites, as gases and aerosols are transported by wind and interact. For instance, fires in the PNW region have been found to significantly impact tropospheric composition in the North Atlantic ocean basin (Lapina et al., 2006), indicating that the fires play a large role in determining the tropospheric composition throughout much of the Northern Hemisphere. Notably, wildfires can cause large increases in the concentrations of carbon monoxide (CO), ozone (O_3), nitrogen oxides (NO_X), and fine particulate matter ($PM_{2.5}$), all of which negatively affect air quality (Cheng et al., 1998; Phuleria et al., 2005, e.g.). Given that anthropogenic emissions influence air pollution across states to produce negative health outcomes (Dedoussi et al., 2020), additional research on the air quality of regions downwind of wildfires in the Western U.S. is important to understanding how Western fires may affect the quality of life across North America.

The year 2020 gives a glimpse of potential future wildfires in the Western U.S. According to the National Interagency Coordination Center (NICC) (2020), the 2020 United States wildfire season was unique, as neither Alaska nor the Southern regions, two fire-prone areas, contributed as much as usual to the total acreage burned. The area that burned, over 10 million acres, was disproportionately located in California and the Northwest, when compared to other years. In particular, in 2020 there were numerous large fires in California, Colorado, Washington, and Oregon, including the first reported million-acre fire in California, which resulted in extensive damage including fatalities and property loss. Consequently, the Northwest, Northern California, and Southern California were both significantly above the ten-year average acreage burned, at 223, 611, and 446 percent respectively, which shattered records for the region (National Interagency Coordination Center (NICC), 2020). Additionally, as the Western U.S. becomes increasingly fire-prone, the impact of its fire events on air quality of the surrounding regions will continue to grow (Ford et al., 2018).

In this study we investigate the recent extreme 2020 wildfires in the Western U.S. region, particularly in the states closest to the West Coast, and how wildfire emissions affected atmospheric composition. Section 2 describes the modeling framework, measurements of trace gases, and analysis methods. Section 3.1 presents an analysis of emissions from the 2020 season in the context of previous seasons. Next, Section 3.2 explores the large-scale impacts of the Western U.S. fires on CO in the atmospheric column 3.2.1 and at the surface level 3.2.2. Section 3.3 analyzes the case study of Boulder, Colorado, in order to identify transported fire pollution in another region with high fire activity. Finally, Section 4 considers the implications of our findings. We conclude in Section 5.

2. Methodology

2.1. Model

2.1.1. CAM-chem

The Community Atmosphere Model version 6 with chemistry (CAM-chem), a component of the Community Earth System Model version 2 (CESM2), simulates global tropospheric and stratospheric composition and is developed by the National Center for Atmospheric Research (NCAR) (Danabasoglu et al., 2020). We use the current version with the updated Model for Ozone and Related chemical Tracers (MOZART-TS1) chemistry mechanism (Emmons et al., 2020; Tilmes et al., 2019). Simulations are performed on 32 vertical layers reaching from the surface to an altitude of ~45 km, with a 0.95° latitude by 1.25° longitude horizontal resolution.

We used a nudging meteorological scheme, recommended by Otte (2008), with Modern-Era Retrospective analysis for Research and Applications, Version 2 (MERRA2) meteorology regridded to the CAM-chem 32 levels, and using the FCnudged component set (Gaubert et al., 2020). The temperature, zonal wind, and meridional wind variables (*T*, *u*, and *v*) in the model were nudged towards the large-scale atmospheric dynamic conditions provided by MERRA2 at 25% every three hours.

Emissions are set to the same grid as the model (0.95° × 1.25°) and include primary emissions of trace gases and aerosols from different sources. Copernicus Atmosphere Monitoring Service Global Anthropogenic Emissions Version 5.1 (CAMS-GLOB-ANT v5.1) are used for anthropogenic emissions (Granier et al., 2019). Additional emissions (from soil, oceans, volcanoes) are as described in Emmons et al. (2020). Biogenic emissions are calculated online in the Community Land Model (CLM) using the Model of Emissions of Gases and Aerosols (MEGAN2.1) algorithms (Guenther et al., 2012), which is coupled to CAM-chem. Fire emissions are described below.

2.1.2. Fire emissions from QFED

Fire emissions were used to analyze the 2020 wildfire season as well as represent fire activity in the CAM-chem model. We used the Quick Fire Emissions Database version 2.5_r1 (QFED) to provide fire emissions (Koster et al., 2015), which are created from satellite measurements of Fire Radiative Power (FRP). The QFED inventory was prepared for use in CAM-chem by multiplying the QFED CO_2 emissions by emission ratios collected from the Fire Inventory from NCAR (FINN1.5) emission factor tables (Wiedinmyer et al., 2011). Section 3.1 explores the 2020 Western U.S. fire season using QFED, in the context of other years, and is supplemented by information about the fires in California from the California Department of Forestry and Fire Protection (CalFire; https://www.fire.ca.gov/stats-events/).

2.1.3. Sensitivity experiment design

Following a model spin-up of the first six months of 2020, we ran three branching cases covering July to December 2020: a control case and two masked cases (Fig. 1). The control case continued simulations using the spin-up configuration, specifically with QFED fire emissions. For the first masked case, the QFED trace gas and aerosol emissions were set to zero in our defined region of the Western U.S. (32.5–49° N, 125–115° W). We chose to mask this Western U.S area, the states closest to the Pacific coast of the U.S., because it is the area of the United States where a disproportionately large number of the 2020 wildfires occurred (National Interagency Coordination Center (NICC), 2020). British Columbia (49–60° N, 125–115° W) was not included in the masked region since it made a relatively small contribution to the overall emissions levels in 2020 (Fig. 3), and it is not under the policy control of the United States.

Our second masked case included setting fire emissions to zero only over the southern section of Western U.S. (32.5–42° N, 115–125° W), which we define as the masked CA case. We ran the masked CA case in order to analyze the contribution of fires mainly in California compared to the entire Western region to atmospheric composition. We subsequently refer to the masked Western U.S. case as the masked case, and the case with only the southern half of the Western U.S. masked as the masked CA case. We analyze simulation output in four regions: Northwest (NW, 42–49° N, 115–125° W), California (CA, 32.5–42° N, 115–125° W), Central (35-49° N, 110-95° W), Northeast (NE, 41-to 53° N, 95-74° W) (Fig. A.1). The regions of analysis considered in this paper correspond with Buchholz et al. (2022) who found that these regions captured areas important for positive trends in atmospheric CO amounts related to North American wildfire.

2.2. Measurements

2.2.1. Satellite-based column CO

We evaluate CAM-chem CO against column CO from the Measurement of Pollution in the Troposphere Version 9 joint thermal infrared and near infrared retrievals (MOPITT-V9J), which is a gas correlation spectrometer carried by the NASA/Terra satellite that was launched in December 1999 (Drummond et al., 2010). MOPITT provides global coverage approximately every 3 days and observes the Earth in swaths

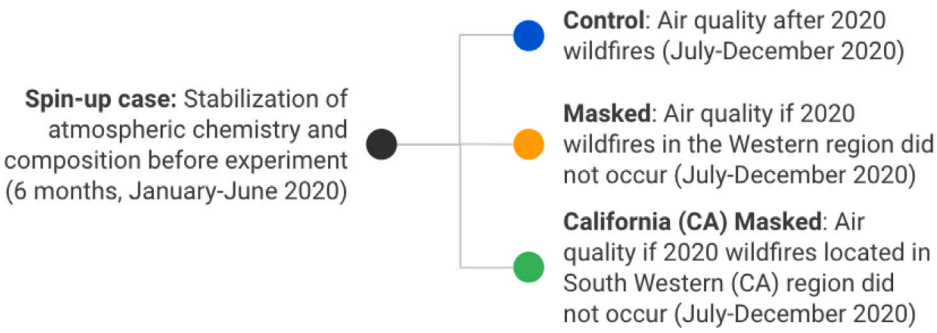

Fig. 1. A diagram summarizing the CAM-chem simulation experiments performed in this study. The regions associated with masking are shown in Fig. 3.

with a width of 640 km with a spatial resolution of 22 km at nadir and an overpass time of 10:30 am and pm local standard time (Drummond et al., 2010). MOPITT vertical profiles have been validated against aircraft and ground-based column measurements (Tang et al., 2020; Deeter et al., 2019; Hedelius et al., 2019; Buchholz et al., 2017), with bias of ~10% (Deeter et al., 2019) in V-8 and improved bias in V-9 (Deeter et al., 2021, 2022). For our comparison, we use the MOPITT-V9 regridded 1° × 1° level 3, monthly-average CO column product (DOI: 10.5067/TERRA/MOPITT/MOP03JM.009) for August, September, and October, 2020; the months with maximum Western U.S. wildfire activity. Modeled CO profiles are convolved with measurement averaging kernels and a priori to account for observational sensitivity in the modeled column CO, as described in Buchholz et al. (2021).

2.2.2. Boulder ground-based column measurements

Direct solar infrared (IR) absorption spectra for 2020 during cloud-free days were measured in Boulder, Colorado using a Bruker HR-FTIR Spectrometer (FTS). The instrument is operated as part of the Network for Detection of Atmospheric Composition Change (NDACC, http://ndacc.org) (Hedelius et al., 2019; De Maziére et al., 2018) and spectra are recorded and analyzed following the standards set by the Infrared Working Group (IRWG, https://www2.acom.ucar.edu/irwg) of the NDACC. Retrievals are performed using the SFIT4 v0.9.4 spectral analysis code, which accounts for pressure and temperature dependence of constituent absorption features and solar line of sight to derive vertical profiles and corresponding total columns. The vertical profiles are used to calculate air mass weighted tropospheric mixing ratio to compare values to the CAM-chem model simulations. We compare CO, hydrogen cyanide (HCN), formaldehyde (CH_2O) and ozone (O_3). Coincident dates of modeled vertical profiles of the nearest pixel to the FTIR are smoothed with the FTIR averaging kernels and a priori vertical profiles to account for the FTIR altitude sensitivity. See Ortega et al. (2021) for more information about the collection site, data retrieval, and analysis methods.

3. Results

3.1. The 2020 Western U.S. fire season

CO is produced during incomplete combustion, and is emitted in large quantities from wildfires. Therefore, we use CO emissions and observed atmospheric concentrations to investigate spatiotemporal properties of the 2020 wildfire season. In this section we use QFED fire emissions which are based off of satellite measurements (see Section 2.1.1 for more details) and therefore are related to the observed fires; fires that were not large enough to be observed by satellites are not accounted for. By giving a sense of how 2020 compared to other years, this analysis provides a basis for estimating air quality impacts from fires in the Western U.S. relative to previous years. We also use this analysis to justify our choice of the masked regions in our model sensitivity experiments.

Overall, the 2020 wildfire season in the Western U.S. was unprecedented. The U.S. wildfires produced emissions that exceeded the average yearly emissions between 2001 and 2019 (Table 1) and were the highest in the region for any single year since 2001 (Fig. 2a, Fig. 2b). In particular, wildfire emissions in some parts of the Western U.S. region were more than 5 times (500%) the average from 2001–2019 (Fig. 3b), with the whole Western U.S. region releasing about three times the average emissions (Table 1). The Western U.S. accounted for more than half of the U.S. wildfire emissions in 2020 (Fig. 2b), exceeding the contribution from other areas of the country (Fig. 3a), and the majority of the Western U.S. emissions originated in California (Table 1).

Consistent with previous years, the Western U.S. fire season in 2020 occurred in the later and warmer months of the year (Fig. 2a) with most emissions in August and September. However, the fire season in 2020 began and continued later than in previous years, since fire emissions remained high into the fall of 2020 whereas they generally decreased after late summer in previous years (Fig. 2a). In fact, U.S. fire emissions continued increasing until around October in 2020 while previous years generally exhibit a leveling trend by late August (Fig. 2b).

In addition, using data obtained from the California Department of Forestry and Fire Protection (CalFire; https://www.fire.ca.gov/stats-events/), we analyzed the fire ignitions over the state of California. While this analysis does not correspond to all of the fires in our Western U.S. region, it is representative of a majority of the CA region where a large proportion of the Western U.S. fires occurred. We determined that the number of fires during July to October increased in 2020 (7244 fires in California) compared to the 2001–2019 average (average of 6620 fires in California). This increase can be attributed in part to an increase in fires with identified anthropogenic causes, including arson, campfires, electrical power, and vehicles (Fig. 4a). However, despite the increases in fires due to human causes, the majority of burned acreage in 2020 was due to fires ignited by lightning (Fig. 4b).

3.2. Large-scale impacts of 2020 wildfires on atmospheric composition

3.2.1. Fires and columnar CO

We begin with an analysis of atmospheric column amounts because they allow for the identification of pollution transport across the U.S. Specifically, the intermediate lifetime of CO makes it a valuable tracer for tracking atmospheric transport from large sources such as wildfire (Chandra et al., 2016; Sodemann et al., 2011; Edwards et al., 2004).

We observe large satellite-measured column amounts of CO over North America in August through October (MOPITT-V9, Fig. 5, row 1). In September, particularly high CO was observed in the western part of the country nearest the wildfires, and also over the central and eastern regions, likely due to transported fire emissions. Model simulations can help attribute high CO to influence from wildfires.

Modeled CO shows similar spatial distribution and temporal evolution of the CO from August to October as the measurements, although

Table 1
Regional yearly sum of QFED fire emissions in 2020 compared with the 2001–2019 average.

	Western U.S. 32.5°–49° N 115°–125° W		California 32.5°–42° N 115°–125° W		Contiguous U.S. 25°–50° N 66°–125° W	
Species	2020	2001–2019 Mean	2020	2001–2019 Mean	2020	2001–2019 Mean
CO (Tg)	12.865	4.536	9.942	2.250	23.067	13.327
NO_X (Tg N)	0.140	0.055	0.103	0.028	0.312	0.203
BC[a] (Tg C)	0.078	0.030	0.063	0.019	0.145	0.081
POM[b] (Tg C)	1.166	0.401	0.907	0.197	1.990	1.115
IVOC[c] + SVOC[d] (Tg C)	0.930	0.323	0.722	0.160	1.617	0.916

[a]Black Carbon.
[b]Particulate Organic Matter.
[c]Intermediate-Volatility Organic Compounds.
[d]Semivolatile Organic Compounds.

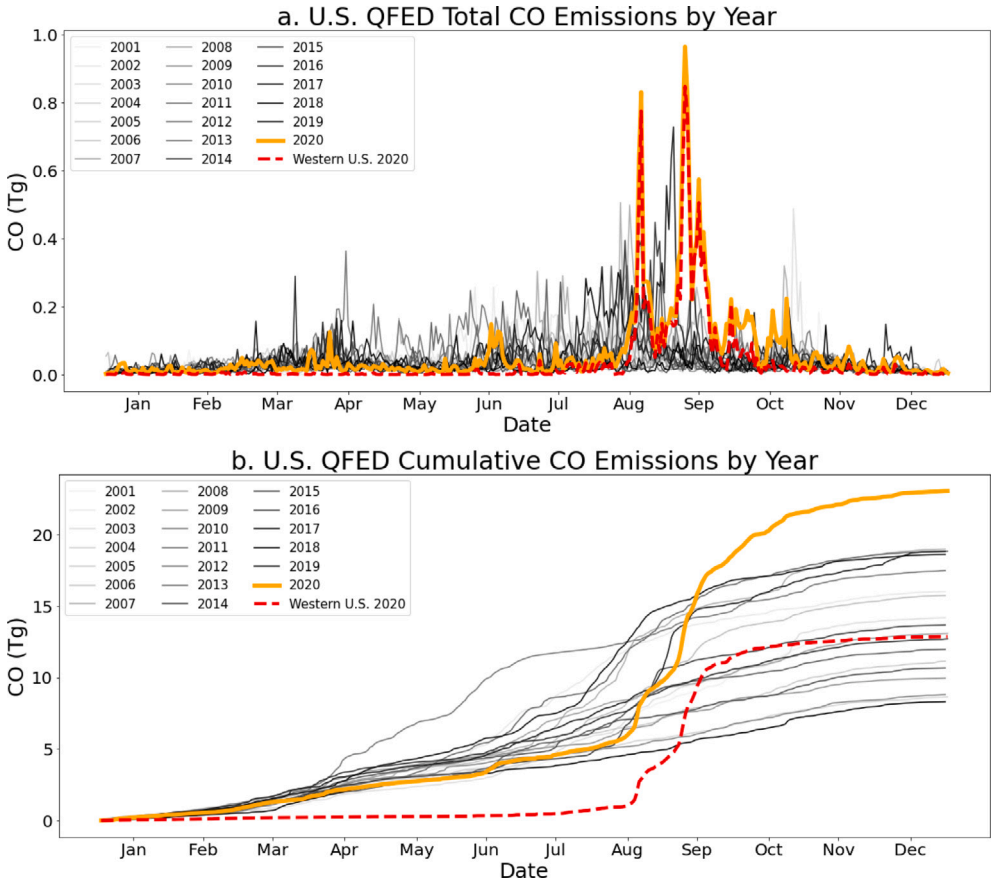

Fig. 2. a. Timeseries of QFED wildfire CO emissions as a daily area-weighted sum over the U.S. (25°–50° N, 66°–125° W) shown for each year 2000 to 2020. b. Cumulative timeseries of QFED wildfire CO emissions as a daily area-weighted sum over the U.S. shown for each year 2000 to 2020. The year of interest, 2020, is highlighted in orange. Western U.S. (32.5°–49° N, 115°–125° W) emissions in 2020 are shown in dashed red as a comparison, and correspond with the area defined in orange in Fig. 3. (For interpretation of the references to color in this figure legend, the reader is referred to the web version of this article.)

with lower magnitudes (Fig. 5, row 2). CAM-chem is known to underestimate CO when compared with MOPITT, with larger differences in the Northern Hemisphere than the Southern Hemisphere (Emmons et al., 2020). In general, we also find the observed CO values are higher than the control simulation by about 20% to 30% (Supplementary Fig. A.2), which has been attributed in previous studies to low estimates of anthropogenic and fire emissions (Wang et al., 2021; Pan et al., 2020; Bowman et al., 2009; Emmons et al., 2020, e.g.). Other possible factors for the model-measurement mis-match are spatiotemporal sampling differences and model parameterizations. Specifically, CAM-chem output shown here are average values from all times of day (including at night) while MOPITT overpasses at approximately 10:30 am (see 2.2.1). A more rigorous model evaluation could focus on the model output data at the time and location of the satellite data and remove days from the model output where there is missing data in MOPITT. However, our goal is to estimate large-scale impacts from the Western U.S. fires using the model rather than quantify measurement-model mis-match. Hence, we show our model results are broadly consistent with other studies that show CAM-chem underestimates CO. Finally, CAM-chem emissions are emitted at the surface and rely on model physics to be vertically transported, potentially underestimating plume rise compared to the real world (Emmons et al., 2020). Smoke plume rise in the real world can cause emissions to travel upwards into higher levels of the atmosphere at a faster rate, where they may move more quickly away from their source (Guan et al., 2008) and atmospheric loss can be slower. A study over CONUS showed plume rise was

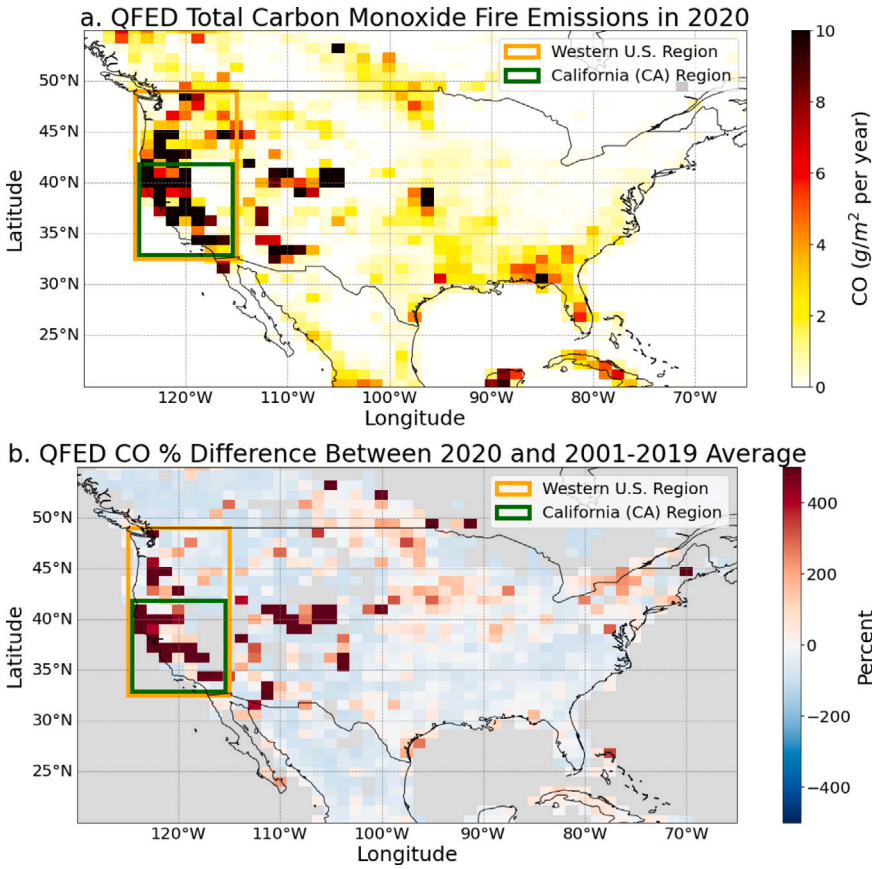

Fig. 3. a. Map of QFED wildfire CO emissions in 2020. b. Map of percent difference between QFED wildfire CO emissions in 2020 and the average QFED wildfire CO emissions in 2001–2019. Masked regions for the model sensitivity simulations are shown in orange and green. (For interpretation of the references to color in this figure legend, the reader is referred to the web version of this article.)

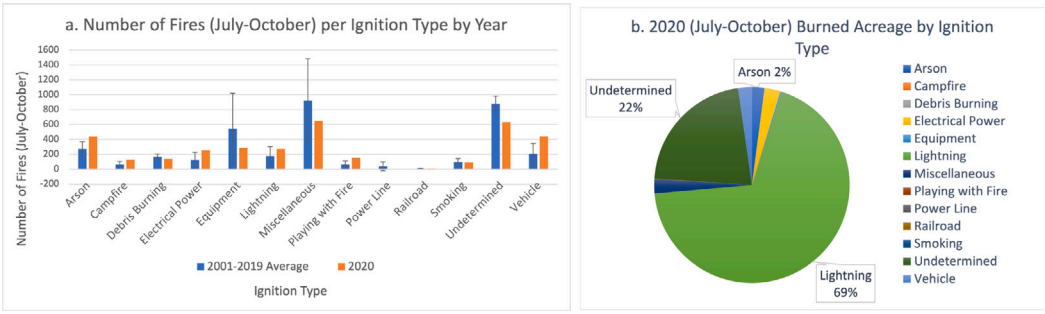

Fig. 4. a. A bar chart comparing the number of fires in California per ignition type in July–October 2020 with the average for 2001–2019. b. A pie chart of burned acreage in California by ignition type in July–October 2020. The data was obtained from a special request to the California Department of Forestry and Fire Protection (https://www.fire.ca.gov/stats-events/).

particularly important for modeling long-range transport of fire-emitted pollutants (Tang et al., 2022). The combination and complexity of these sources of uncertainty, as discussed in Pan et al. (2020) and Liu et al. (2020), means that it is extremely difficult to quantify an estimate of uncertainty for model output. Future research will aim to quantify the individual and combined uncertainty in modeled atmospheric composition results from wildfire sources.

Acknowledging these factors that may contribute to differences between the measured data and model output, we still observe that the spatial distribution and temporal evolution of the CO between the control simulation and measurements are generally consistent (Fig. 5). Notably, in both the control model and measurement data sets, we observe the highest average CO concentration values in August and September. Therefore, the model allows us to compare possible scenarios with and without emissions from fires to consider effects on pollution transport with the caveat that our results likely underestimate the impact of fire emissions on CO.

Fig. 6 presents the percent difference in monthly CO column between the simulations with and without Western U.S. fire emissions from August to October, calculated as control minus masked relative to the control simulation. Results can be interpreted as the contribution of Western U.S. fires to the total amount of CO in each month. It is clear that the inclusion of Western U.S. fires resulted in higher amounts of CO, particularly in the western half of the country for all three months, with fires contributing 50% or more to the total CO at some locations. We also observe smaller contributions of ~5%–10% to CO for regions of the country downwind of the wildfires. In September, the model suggests substantial transport to the central region of the U.S. (~20%) and in October, the whole North American domain shows small

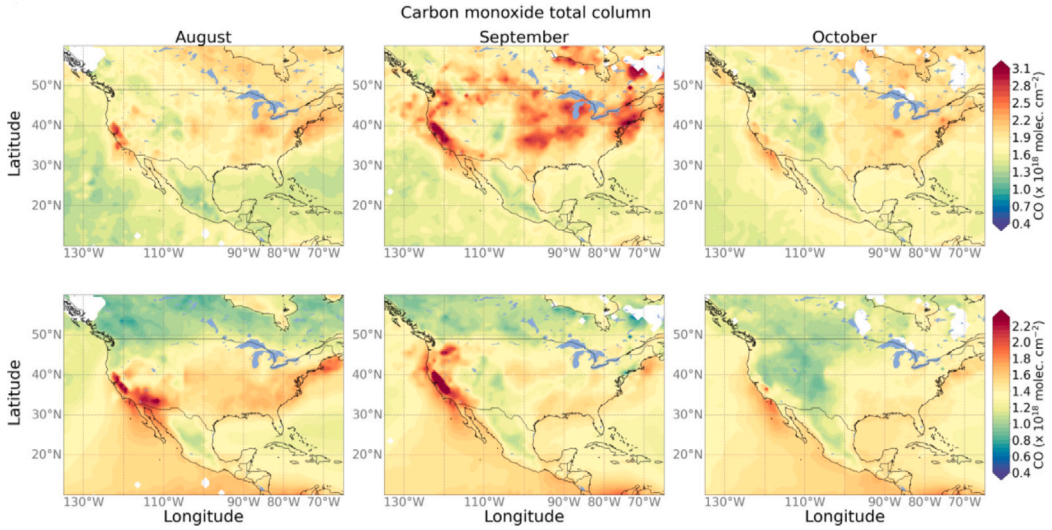

Fig. 5. Average monthly MOPITT CO column amounts covering August to October are shown in the first row. CAM-chem monthly average CO column from the control simulation for August to October are shown in the second row. Note the different colorbar ranges between rows.

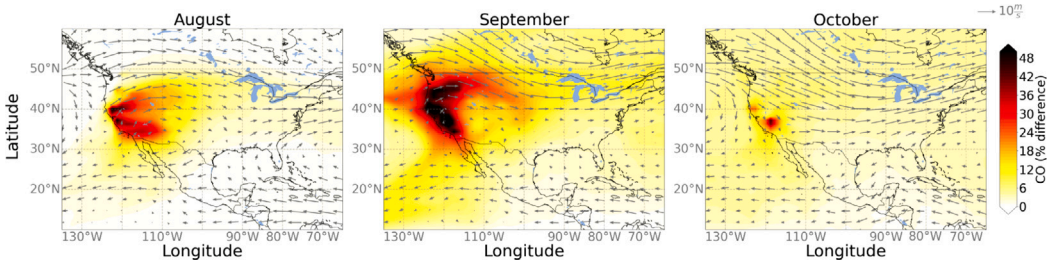

Fig. 6. Monthly average CO column percent difference between simulations with and without Western U.S. fire emissions. Average wind vectors are denoted by gray arrows for the approximate 750 hPa model layer (layer 23).

increases (~5%) due to fire emissions, suggesting that fire activity in the Western U.S. has an impact on the background levels of pollution across the whole of North America. Aggregated analysis shows the largest average increase in column CO over the Contiguous U.S. occurs in September, at 14.5% of CO resulting from fires (Table 2). By November the Western U.S. fire emissions are atmospherically well mixed as observed by CONUS and the Northern Hemisphere seeing equivalent contribution to CO from the Western U.S. fire emissions. A residual impact on the whole Northern Hemisphere remains in November and December, with approximately 2% CO contributed from the Western U.S. fires.

Furthermore, the average wind vectors on Fig. 6 demonstrate that while dominant transport in the free troposphere for all three months (~ 750 hPa) is westerly (transport to the east), August shows more northeastward transport from Southern California than September or October. These transport differences may have implications for locations downwind of the fire, such as Boulder, Colorado, which we discuss in Section 3.3.

3.2.2. Model estimation of wildfire impacts on surface level atmospheric composition

We focus on analyzing modeled fire impacts on surface level O_3 and $PM_{2.5}$ values since they are two pollutants from fires that have been shown to have negative health effects (Voulgarakis and Field, 2015; Finlay et al., 2012, e.g.). We assess surface values averaged in four regions of the U.S., to investigate areas both local and downwind from the Western U.S. fires (See Section 2.1.3 and Fig. A.1). Box plot analysis shows the distribution of O_3 and $PM_{2.5}$ averages and extremes in each geographical region between August and October (Fig. 7). The largest changes in average values due to fire emissions occurred for O_3 and $PM_{2.5}$ in the CA and NW regions (Fig. 7). This finding is consistent with previous studies that have found that smoke aerosols cause significant pollution changes over the western half of the U.S. between high and low fire years (Xue et al., 2021).

Table 2
Average percent change in column CO due to Western U.S. fire emissions.

Month	~CONUS (25°–50° N, 66°–125° W)	Northern Hemisphere (0°–90° N, 0°–360° E)
Jul	0.5	<0.1
Aug	6.5	0.6
Sep	14.5	3.2
Oct	4.9	3.4
Nov	2.4	2.4
Dec	1.7	1.7

We further considered time series of daily regional averaged surface O_3 and $PM_{2.5}$ amounts in order to investigate how atmospheric composition impacts change over the fire season. The CA region experienced three fire-driven peaks in average O_3 between August and October (Fig. 8a), while the NW region only experienced one peak in average O_3 (Fig. 8b). For the CA region, August and September mean O_3 peaks are of the same magnitude (~80 ppb). However, since the masked CA simulation only differs from the masked simulation in California in September, the sensitivity experiments show that the August peak was driven by local California fire emissions, while the September peak experienced some contribution from fires in the NW region reflecting

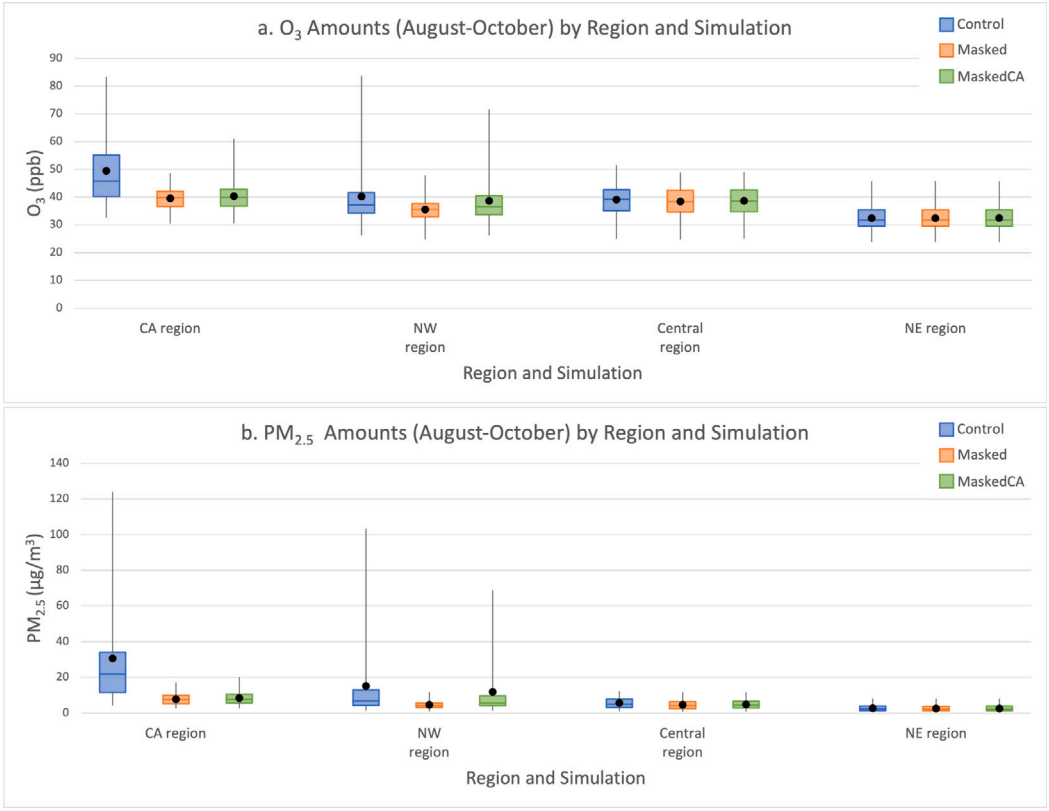

Fig. 7. Box plots of average surface O_3 (a) and $PM_{2.5}$ (b) amounts between August and October for the CA, NW, Central, and NE regions for each simulation. Boxes display 25th percentile, median, and 75th percentile values, while whiskers extend to minimum and maximum values. Mean values are marked by points.

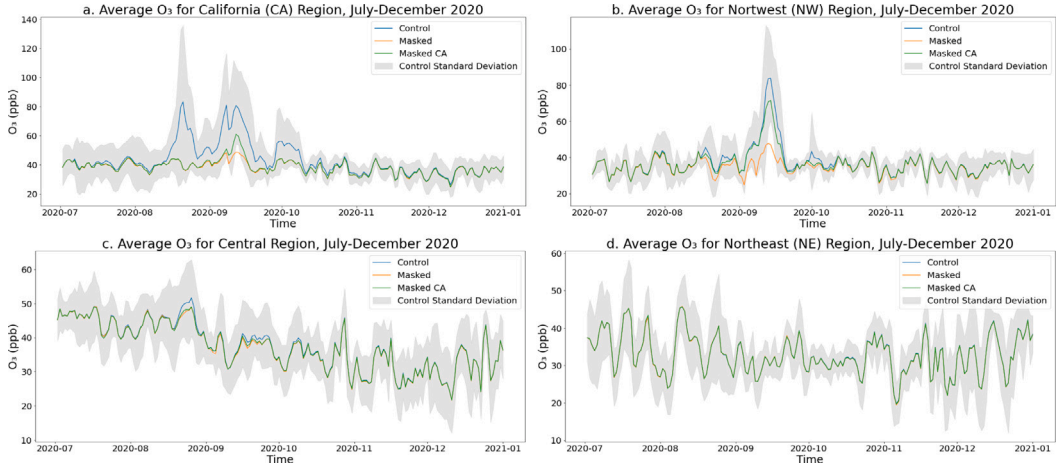

Fig. 8. Timeseries of O_3 amounts in the CA, NW, Central, and NE regions for each simulation. Each timeseries also displays the standard deviation for the control simulation. Each *x*-axis tick corresponds to the first day of each month.

pollution transport from the NW into CA. Similarly, the NW shows some contribution from California fires in the September peak, which is above 80 ppb, but there are no transported impacts from the South during August, indicating north–south mixing and potential pollution recirculation was strongest in September. The Central region (Fig. 8c) experienced some impacts on average O_3 in August and September due to the Western U.S. fires, showing the potential for transported fire emissions to impact surface air quality downwind; however, the magnitude of enhancements never exceeded ~5 ppb. In comparison, according to CAM-chem, the Western fire emissions minimally impact O_3 amounts in the NE region (Fig. 8d).

Similar mean regional time series analysis for $PM_{2.5}$ show analogous results to O_3, and illustrates that surface $PM_{2.5}$ variability is dominated by the local region emissions more than transported emissions (Fig. 9). California fires were responsible for all three $PM_{2.5}$ enhancements in California, as seen by masking of emissions in the California region producing equivalent results to masking the whole Western region. In September, transport northward from California to the NW region occurred for $PM_{2.5}$, but there was minimal transport southward. In the Central region, we observe the influence from Western U.S. fire emissions in August through October, with substantial influence in mid August and mid September (Fig. 9c). While the peaks in the Central region are small compared to the magnitude of the peaks in the CA and NW regions, it is interesting to note that the first transported peak in late August/early September is primarily due to fires in CA

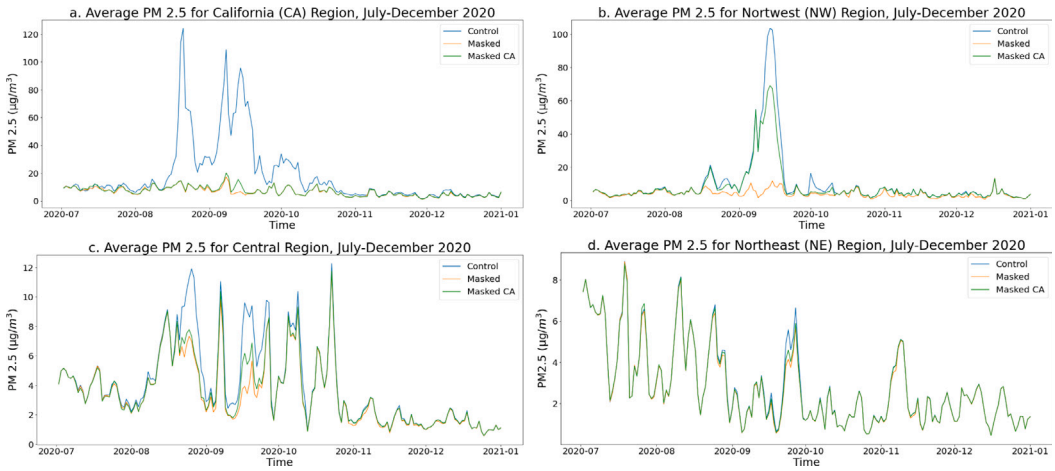

Fig. 9. Time series of regional average $PM_{2.5}$ amounts for the CA (a), NW (b), Central (c), and NE (d) regions for each simulation.

while the second peak in late September is a result of fires in both CA and the NW. In comparison, there is not much change in average values in the NE region, with generally lower $PM_{2.5}$ values overall and potentially very small transported impact during late September. Further, we analyzed maximum $PM_{2.5}$ values (Supplementary Fig. A.3) and found a noticeable decrease in maximum $PM_{2.5}$ values in CA and NW regions between the control and masked simulations, while the central and NE regions show little change in extremes.

3.3. Boulder case study: identifying transported fire pollution

For a localized case study of transported pollution, we compared our control simulation with column measurements from the FTS instrument in Boulder, Colorado, a location in our defined Central region. It is important to note that Colorado also experienced an extreme fire season in 2020, with CO emissions from wildfires reaching above 4 times (400%) of the 2001–2019 average values (Fig. 3). Therefore, this case study allowed us to consider the relationships between regions with high fire activity.

Overall, we see similar temporal patterns between the observed and modeled tropospheric column amounts of CO, HCN, CH_2O and O_3 (Fig. 10). Observed values of CO, HCN and CH_2O were substantially above the 2010–2019 average from August to October, due to a combination of local and transported fire pollution, that we can use the model to help distinguish.

Similar to comparisons with satellite measurements in Section 3.2.1, the control simulation underestimated column CO in Boulder, Colorado; while the simulation and FTS measurements showed similar extremes and variability during the fire season, the simulation consistently underestimated CO values outside of the fire season (Fig. 10). This underestimation has been observed in other studies and attributed to missing anthropogenic emissions (Ortega et al., 2021; Emmons et al., 2020; Gaubert et al., 2017, e.g.). In addition to factors discussed for the model-measurement mis-match in Section 3.2.1, CAM-chem output shown here is an average of values from all times of day (including at night) while the FTS is a clear sky solar occultation measurement instrument so it does not record measurements overnight and often not in the late afternoon (Ortega et al., 2021). Additionally, the viewing angle of the FTS may not match the model vertical column above Boulder, and spatial dilution in the model (comparing a 1-degree box with a single path through the atmosphere) may also contribute (Ortega et al., 2021). Specifically, it is also important to note that in this analysis we are comparing a rather coarse resolution model to a point measurement in an area with complex terrain and meteorology and diverse emission sources. Even with the comparison of columns, the near-surface concentrations will dominate the observed column amounts for most of the species, which the coarse model may have difficulty representing completely.

Model sensitivity experiments are useful for identifying local versus transported fire impacts in the Boulder FTS record. CO column amounts exhibit similar temporal variability between the FTS measurements and the control simulation (Fig. 10a). Further, some of the largest peaks are of similar magnitude and show no difference between the FTS, control, and masked time series, suggesting that local fires were the cause of increased CO amounts. In comparison, there are two peaks, mid-August and mid-September, that show differences between the control and masked simulations, indicating that transported Western U.S. fire pollution was the cause of increased CO amounts. During these two peaks, transported CA wildfire pollution contributed the most to the modeled CO enhancements.

HCN is overestimated by the model (Fig. 10b), which was previously shown when using QFED biomass burning emissions in Ortega et al. (2021). However, seeing as HCN is predominantly a fire tracer, the similar temporal pattern between modeled CO and HCN for August through October supports that all the higher values in 2020 are due to fire emissions, be it local or transported. Mid-August and mid-September transported influence is also reflected in the modeled HCN. Regarding CH_2O, the model shows little difference between the three simulations at Boulder (Fig. 10c). Although modeled CH_2O compares very well with the FTS, there are two measured peaks that are not captured by the control model – one in mid-August and another in mid-September – that coincide with transported fire emissions for the other species. The absent CH_2O peaks during the transported events imply that modeled CH_2O is mainly impacted by local fire and suggests a missing process in CAM-chem, such as too much chemical destruction or a missing chemical source in the modeled transported plume.

Finally, the different temporal pattern of O_3 at Boulder compared to the other three species shows the complexity of processes that contribute to atmospheric O_3. Modeled O_3 seems slightly overestimated compared to the Boulder FTS during the fire season (Fig. 10d), which is consistent with a well known high bias for O_3 in CAM-chem (Emmons et al., 2020). The model O_3 suggests some enhanced O_3 concentrations during the fire season, additionally with some influence from transported fire emissions at times coincident with the transported peaks in the CO time series. Although difficult to determine, there is potentially associated O_3 enhancements observed in the measurements during the transported events, but fire plumes are known to have variable O_3 production. A more thorough plume-by-plume analysis at higher temporal resolution is planned for future work.

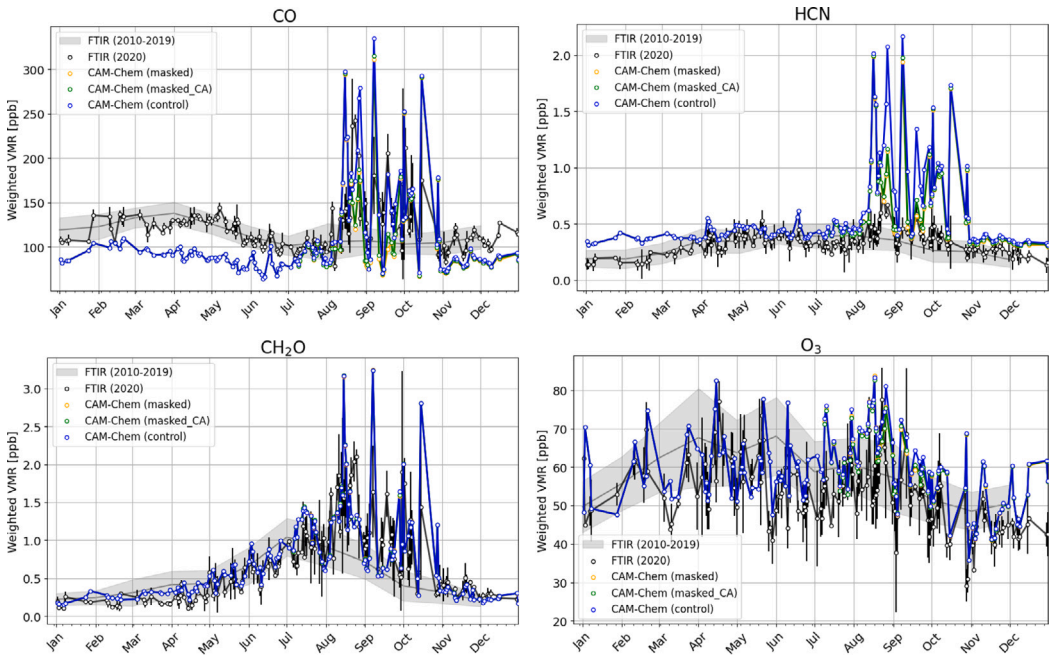

Fig. 10. Tropospheric weighted mixing ratios of CO (a), HCN (b), CH_2O (c), and O_3 (d) from the Boulder/NCAR FTS in 2020 (black) compared to the 2010–2019 average (gray). Co-located column amounts from the three CAM-chem simulations (blue, green, orange) are shown as comparison.

4. Discussion

The 2020 Western U.S. wildfire season demonstrated an extreme in the trend of increasing number of wildfires and burned area compared to previous years (Li and Banerjee, 2021), including an extreme for emissions as discussed in Section 3.1. While the number of human-induced fires increased (Fig. 4), consistent with the findings of Li and Banerjee (2021), we found that fires caused by lightning accounted for a large majority of burned acreage in 2020. In fact, four of the five largest fire complexes in California (August Complex, SCU Lightning Complex, Creek Complex, LNU Lightning Complex, and North Complex) in 2020 were ignited by lightning (the Creek Complex is still under investigation) and are responsible for the increase in burned area as compared to previous years (California Department of Forestry and Fire Protection, https://www.fire.ca.gov/media/4jandlhh/top20_acres.pdf). This suggests that the increase in burned acreage, and consequently fire emissions is potentially linked more strongly with changes in climate, dryness, and weather patterns than direct human activity. Future research could explore this connection more thoroughly, adding context to the anomalous year of 2020.

Irrespective of the cause, the emissions from the 2020 Western U.S. wildfires were unprecedented, making them an ideal case study for transported pollution. Our findings that Western U.S. wildfires have a much larger effect on health tracers at surface level in the geographic areas closest to the fires themselves are not surprising. Health implications of our findings must be considered in the context of model bias, especially since the global coarse resolution model is not necessarily suited for estimating health impacts. For O_3, the EPA exposure limit is 70 ppb on an 8-hr period (Environmental Protection Agency, https://www.epa.gov/criteria-air-pollutants/naaqs-table); therefore, the daily average spikes above 80 ppb caused by fires exceed health limits, even with a ~ 10 ppb model overestimate as seen in the southeastern U.S. in Emmons et al. (2020). Consequently, fires are a major factor in moving O_3 amounts close to or over the health limits in the CA and NW regions during August to October. In contrast, aerosol amounts have been found to be underestimated in the CAM-chem model (Lamarque et al., 2012; Tilmes et al., 2019). The enhancements in surface $PM_{2.5}$ are therefore likely underestimated. The EPA standard of 35 μg m^{-3} for a 24 h exposure is far exceeded in the NW and CA regions due to fires, where our model results show daily average values exceeding 100 μg m^{-3} at times. While average values for the Central and NE regions do not exceed 35 μg m^{-3}, the inclusion of fires does result in increased $PM_{2.5}$ amounts. Therefore, increased fire activity has the potential to cause species to exceed health standards across the country.

Overall, our results align with previous studies. For example, Kang et al. (2014) found that O_3 daytime mixing ratios at measurement sites in the Mid-Atlantic reached maximum values of about 100 ppb due to wildfire smoke transport, while Yang et al. (2022) identified a peak in $PM_{2.5}$ amounts downwind of fires to be 105.5 μg m^{-3} through the combination of model and measurement results, which are similar to differences we discuss. Our results also align with the order of magnitude of O_3 enhancements over North America identified in earlier case studies (Pfister et al., 2006; Lapina et al., 2006).

It is important to note that our study of regional averages as well as monthly and 3-month average values presented in Sections 3.2.1 and 3.2.2 provide only part of the picture of wildfire impacts since potential exceedances are diluted by lower concentrations on other days and at other locations, particularly for downwind locations. Consequently our modeled average changes over a larger spatial scale seem small, even though on one particular hour/day/week at one particular location the magnitudes could be very large, and potentially have a pronounced impact on health and air quality. To illustrate this, we plot the fire-driven modeled changes in the July–December maximum in daily average O_3 and $PM_{2.5}$ for the Eastern half of the country (Fig. 11), which shows substantially larger impacts than the average results presented in Sections 3.2.1 and 3.2.2. East of ~100° W, daily maximum O_3 can be increased up to 5 ppb and $PM_{2.5}$ up to 5 μg m^{-3} due to transported Western U.S. wildfire pollution. Further, a recent study found that health implications in the U.S. are further complicated by public awareness around air quality issues, and saw a majority of observed health effects from Western fires occur for the highly populated Eastern part of the country (O' Dell et al., 2021). In the future, machine learning techniques may be helpful to downscale simulations and estimate surface level pollution amounts at specific air quality monitoring sites (Hung et al., 2021) in order to directly link fire impacts to air quality measurements used in policy making.

Additionally, CAM-chem underestimates average pollutant concentrations for CO (Section 3.2.1) and $PM_{2.5}$ (Lamarque et al., 2012),

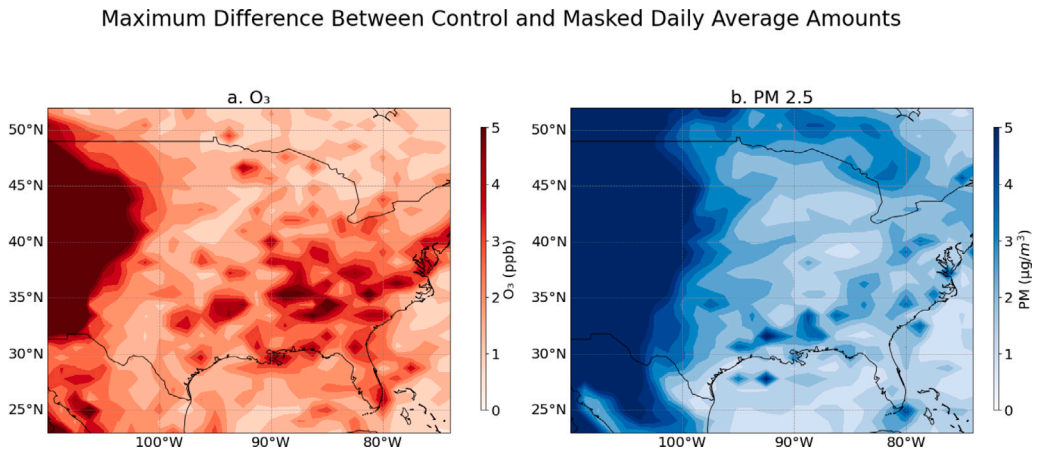

Fig. 11. Maximum differences in daily average surface layer values between control and masked simulations for (a) O_3 (b) $PM_{2.5}$, from July to December.

meaning that our estimated impact on air quality is potentially smaller than the real-world impacts. The model does a better job reproducing CH_2O, and overestimates other species, such as O_3 and HCN (Section 3.3) (Emmons et al., 2020; Ortega et al., 2021, e.g.). This variety in under and overestimation of various species makes it difficult to consider simultaneous exposure, which would allow for a more thorough analysis of cumulative health risks (Dominici et al., 2010). Model limitations leave room for future work to reduce the measurement-model bias.

Overall, our results underscore questions about policy relating to wildfires. For instance, how much should the rest of the country be involved in how Western regions manage their growing number of wildfires? Should lawmakers in the Western regions be considering people in other regions as they make decisions about containing fires? Furthermore, our analysis of California fires in comparison to all Western U.S. fires leaves questions about how policies might differ between California and the Northwest. As Burke et al. (2021) suggest, the growing information about how wildfires affect our air quality may create a different risk and burden for wildfire management. Therefore, wildfire management must evolve, such as through the integration of suppression and prevention, implementation of fuel reduction programs, and sustainable rehabilitation of fire-adapted ecosystems (Steelman and Burke, 2007; Busenberg, 2004).

5. Conclusion

The 2020 wildfire season was unprecedented in the Western U.S., exceeding three times the 2001–2019 average CO emissions. While the largest increase in number of fires in California occurred for some anthropogenic ignition sources, the largest burned area was driven by fires ignited by lightning. Additionally, a temporal difference from previous years, with fires peaking in the early fall rather than the late summer and extending later than previous years, made the year particularly unusual.

Using the Community Atmosphere Model version 6 with Chemistry (CAM-chem), we simulated atmospheric composition with and without fire emissions from the Western U.S. region (32.5–49°N, 115–125°W) to investigate how the 2020 fires affected air quality both locally and at downwind locations. We found that changes in composition between the control and masked simulations differed by regions, with the general pattern of larger changes in daily average concentrations occurring in regions closer to the Western U.S. and decreasing with distance east of the fires. We found two fire-driven enhancements in pollution at Boulder, Colorado occurred during mid-August and mid-September, and identify model deficiencies in reproducing formaldehyde associated with these events. At the surface level, the largest changes in average values of O_3 and $PM_{2.5}$ due to fire occurred in the Western region, reaching up to ~40 ppb and ~120 μg m^{-3}, respectively. Further, through the analysis of two sensitivity studies (removing emissions in the whole Western region versus removing emissions mainly over California) we determined that north–south mixing between the CA and NW regions was strongest in September. Both the NW and CA regions experienced large fires in 2020 so with our sensitivity experiments, we were able to determine the specific impacts of the regions on each other. The Central U.S region saw minor enhancements in surface level amounts of O_3 and $PM_{2.5}$ from fire emissions, indicating that transported fire pollution can reach the surface, and the Northeast region experienced a small transported impact.

Overall, our results leave us to consider how people around the country should be involved or considered in decision making surrounding wildfire burning in the Western region, as well as how much climate change, both through temperature increases and weather extremes, will affect the country's air quality as fires increase.

CRediT authorship contribution statement

I.S. Albores: Data curation, Investigation, Formal analysis, Software, Visualization, Writing – original draft. **R.R. Buchholz:** Conceptualization, Methodology, Formal analysis, Visualization, Writing – reviewing and editing. **I. Ortega:** Data curation, Formal analysis, Visualization, Writing – reviewing and editing. **L.K. Emmons:** Writing – reviewing and editing. **J.W. Hannigan:** Data curation, Writing – reviewing and editing. **F. Lacey:** Writing – reviewing and editing. **G. Pfister:** Writing – reviewing and editing. **W. Tang:** Writing – reviewing and editing. **H.M. Worden:** Writing – reviewing and editing.

Declaration of competing interest

The authors declare that they have no known competing financial interests or personal relationships that could have appeared to influence the work reported in this paper.

Data availability

Data will be made available on request.

Acknowledgments

This material is based upon work supported by the National Science Foundation under Grant No. AGS-1641177, Significant Opportunities for Atmospheric Research and Science (SOARS). Any opinions, findings, and conclusions or recommendations expressed in this material are those of the author(s) and do not necessarily reflect the views of the National Science Foundation.

The National Center for Atmospheric Research (NCAR) is sponsored by the National Science Foundation. We would like to acknowledge high-performance computing support from Cheyenne (http://dx.doi.org/10.5065/D6RX99HX) provided by NCAR's Computational and Information Systems Laboratory, sponsored by the National Science Foundation. The NCAR MOPITT project is supported by the National Aeronautics and Space Administration (NASA) Earth Observing System (EOS) Program. MOPITT is supported by the Canadian Space Agency (CSA), the Natural Sciences and Engineering Research Council (NSERC) and Environment Canada, and the contributions of COMDEV (the prime contractor) and ABB BOMEM. The MOPITT version 9 product used here is publicly available from the NASA Atmospheric Science Data Center (http://dx.doi.org/10.5067/TERRA/MOPITT/MOP03JM.009). The Boulder FTS data (http://dx.doi.org/10.5065/wwxr-tp19, stored at: https://dashrepo.ucar.edu/dataset/ftir.html) used in this publication were obtained as part of the Network for the Detection of Atmospheric Composition Change (NDACC) and are also available through the NDACC website (https://www.ndacc.org) or by request. The NCAR NDACC FTS observation program at Boulder, CO is supported under contract by the National Aeronautics and Space Administration (NASA). We thank the California Department of Forestry and Fire Protection (CalFire, https://www.fire.ca.gov/stats-events/) for providing data on fire activity for 2001–2020 prior to the release of the official 2020 annual Wildfire Activity Statistics Report (Redbook). We thank Simone Tilmes for valuable discussions about our work. We thank NCAR internal reviewer Warren Smith for valuable feedback.

Appendix. Supplemental figures

The figures included in our supporting information (Supplementary Fig. A.1, Fig. A.2, Fig. A.3) provide a visual representation of regions and support values included in our manuscript. In particular, we include a map of our analysis regions which supports the regional analysis included in Section 3.2.1 as well as correlation plots for the differences between the model and MOPITT data which supports the mean biases reported in Section 3.2.2. Additionally, we include $PM_{2.5}$ time series

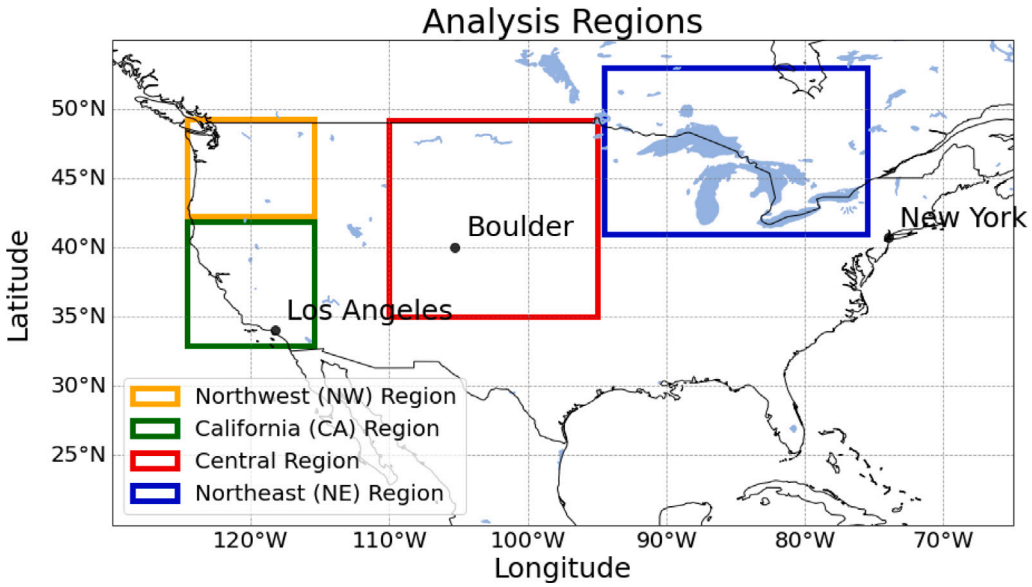

Fig. A.1. A map of the regions used for analysis. The coordinates of each region are included here: Northwest (NW, 42–49° N, 115–125° W), California (CA, 32.5–42° N, 115–125° W), Central (35-49° N, 110-95° W), Northeast (NE, 41-to 53° N, 95-74° W).

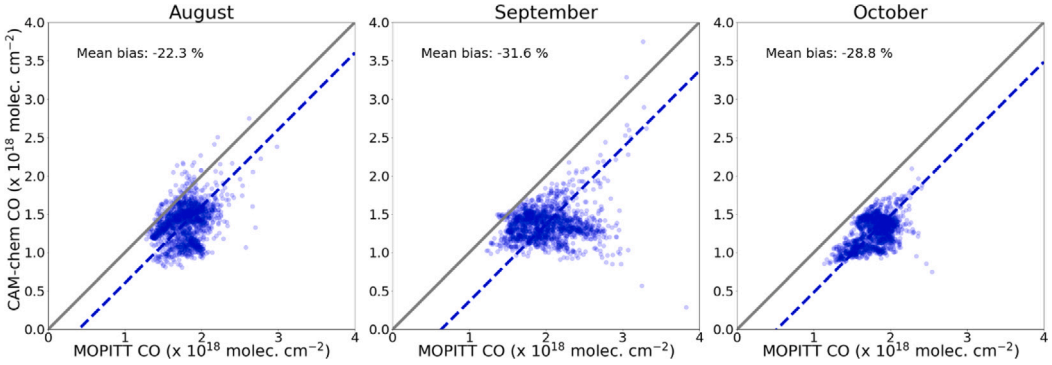

Fig. A.2. Correlation plots of average CO column amounts from the CAM-chem model against MOPITT measurements over the U.S. region by month. The gray solid line represents the theoretical one-to-one ratio while the blue dashed line represents the mean bias observed, with the mean bias value reported in percent relative to the MOPITT mean value for each month in the upper left hand corner of each chart. CAM-chem values were convolved with MOPITT a priori and averaging kernels prior to comparison.

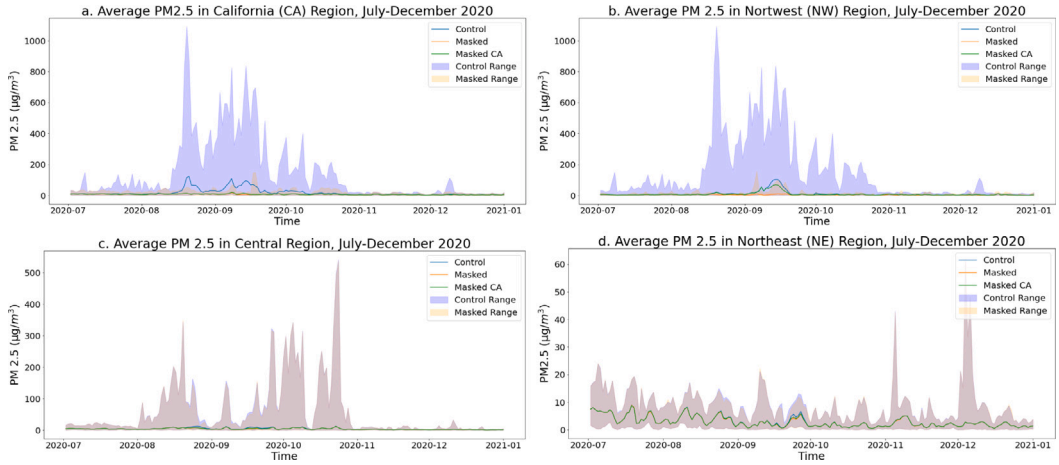

Fig. A.3. Time series of average $PM_{2.5}$ concentration for the CA, NW, Central, and NE regions for each simulation. Each time series also shows the range of $PM_{2.5}$ concentration for the control and masked simulations to compare maximum and minimum values.

that include the range from the control and masked simulation by region, demonstrating how much the Western U.S. wildfires contributed to the maximum $PM_{2.5}$ values in each region.

References

Abatzoglou, J.T., Williams, A.P., 2016. Impact of anthropogenic climate change on wildfire across western US forests. Proc. Natl. Acad. Sci. 113 (11770), http://dx.doi.org/10.1073/pnas.1607171113, URL: http://www.pnas.org/content/113/42/11770.abstract.

Bowman, D.M.J.S., Balch, J.K., Artaxo, P., Bond, W.J., Carlson, J.M., Cochrane, M.A., D' Antonio, C.M., DeFries, R.S., Doyle, J.C., Harrison, S.P., Johnston, F.H., Keeley, J.E., Krawchuk, M.A., Kull, C.A., Marston, J.B., Moritz, M.A., Prentice, I.C., Roos, C.I., Scott, A.C., Swetnam, T.W., van der Werf, G.R., Pyne, S.J., 2009. Fire in the Earth System. Science 324 (481), http://dx.doi.org/10.1126/science.1163886, URL: http://science.sciencemag.org/content/324/5926/481.abstract.

Buchholz, R.R., Deeter, M.N., Worden, H.M., Gille, J., Edwards, D.P., Hannigan, J.W., Jones, N.B., Paton-Walsh, C., Griffith, D.W.T., Smale, D., Robinson, J., Strong, K., Conway, S., Sussmann, R., Hase, F., Blumenstock, T., Mahieu, E., Langerock, B., 2017. Validation of MOPITT carbon monoxide using ground-based Fourier transform infrared spectrometer data from NDACC. Atmos. Meas. Tech. 10, 1927–1956. http://dx.doi.org/10.5194/amt-10-1927-2017, URL: https://amt.copernicus.org/articles/10/1927/2017/, publisher: Copernicus Publications.

Buchholz, Rebecca R., Park, Mijeong, Worden, Helen M., Tang, Wenfu, Edwards, David P., Gaubert, Benjamin, Deeter, Merritt N., Sullivan, Thomas, Ru, Muye, Chin, Mian, Levy, Robert C., Zheng, Bo, Magzamen, Sheryl, 2022. New seasonal pattern of pollution emerges from changing north american wildfires. Nature Commun. 13 (1), 2043. http://dx.doi.org/10.1038/s41467-022-29623-8, URL: https://doi.org/10.1038/s41467-022-29623-8.

Buchholz, R.R., Worden, H.M., Park, M., Francis, G., Deeter, M.N., Edwards, D.P., Emmons, L.K., Gaubert, B., Gille, J., Martınez-Alonso, S., Tang, W., Kumar, R., Drummond, J.R., Clerbaux, C., George, M., Coheur, P.F., Hurtmans, D., Bowman, K.W., Luo, M., Payne, V.H., Worden, J.R., Chin, M., Levy, R.C., Warner, J., Wei, Z., Kulawik, S.S., 2021. Air pollution trends measured from Terra: CO and AOD over industrial, fire-prone, and background regions. Remote Sens. Environ. 256, 112275. http://dx.doi.org/10.1016/j.rse.2020.112275, URL: https://www.sciencedirect.com/science/article/pii/S0034425720306489.

Burke, M., Driscoll, A., Heft-Neal, S., Xue, J., Burney, J., Wara, M., 2021. The changing risk and burden of wildfire in the United States. Proc. Natl. Acad. Sci. 118, e2011048118. http://dx.doi.org/10.1073/pnas.2011048118, URL: http://www.pnas.org/content/118/2/e2011048118.abstract.

Busenberg, G., 2004. Wildfire management in the United States: The evolution of a policy failure. Rev. Policy Res. 21, 145–156. http://dx.doi.org/10.1111/j.1541-1338.2004.00066.x, URL: https://onlinelibrary.wiley.com/doi/abs/10.1111/j.1541-1338.2004.00066.x, _eprint: https://onlinelibrary.wiley.com/doi/pdf/10.1111/j.1541-1338.2004.00066.x.

Chandra, N., Venkataramani, S., Lal, S., Sheel, V., Pozzer, A., 2016. Effects of convection and long-range transport on the distribution of carbon monoxide in the troposphere over India. Atmos. Pollut. Res. 7, 775–785. http://dx.doi.org/10.1016/j.apr.2016.03.005, URL: https://www.sciencedirect.com/science/article/pii/S1309104215300167.

Cheng, L., McDonald, K., Angle, R., Sandhu, H., 1998. Forest fire enhanced photochemical air pollution. A case study. Atmos. Environ. 32, 673–681. http://dx.doi.org/10.1016/S1352-2310(97)00319-1, URL: https://www.sciencedirect.com/science/article/pii/S1352231097003191.

Danabasoglu, G., Lamarque, J.F., Bacmeister, J., Bailey, D.A., DuVivier, A.K., Edwards, J., Emmons, L.K., Fasullo, J., Garcia, R., Gettelman, A., Hannay, C., Holland, M.M., Large, W.G., Lauritzen, P.H., Lawrence, D.M., Lenaerts, J.T.M., Lindsay, K., Lipscomb, W.H., Mills, M.J., Neale, R., Oleson, K.W., Otto-Bliesner, B., Phillips, A.S., Sacks, W., Tilmes, S., Kampenhout, L.van., Vertenstein, M., Bertini, A., Dennis, J., Deser, C., Fischer, C., Fox-Kemper, B., Kay, J.E., Kinnison, D., Kushner, P.J., Larson, V.E., Long, M.C., Mickelson, S., Moore, J.K., Nienhouse, E., Polvani, L., Rasch, P.J., Strand, W.G., 2020. The community earth system model version 2 (CESM2). J. Adv. Modelling Earth Syst. 12, e2019MS001916. http://dx.doi.org/10.1029/2019MS001916, publisher: John Wiley & Sons, Ltd.

De Maziére, M., Thompson, A.M., Kurylo, M.J., Wild, J.D., Bernhard, G., Blumenstock, T., Braathen, G.O., Hannigan, J.W., Lambert, J.C., Leblanc, T., McGee, T.J., Nedoluha, G., Petropavlovskikh, I., Seckmeyer, G., Simon, P.C., Steinbrecht, W., Strahan, S.E., 2018. The network for the detection of atmospheric composition change (NDACC): History, status and perspectives. Atmos. Chem. Phys 18, 4935–4964. http://dx.doi.org/10.5194/acp-18-4935-2018, URL: https://acp.copernicus.org/articles/18/4935/2018/, publisher: Copernicus Publications.

Dedoussi, I.C., Eastham, S.D., Monier, E., Barrett, S.R.H., 2020. Premature mortality related to United States cross-state air pollution. Nature 578, 261–265. http://dx.doi.org/10.1038/s41586-020-1983-8.

Deeter, M.N., Edwards, D.P., Francis, G.L., Gille, J.C., Mao, D., Martınez-Alonso, S., Worden, H.M., Ziskin, D., Andreae, M.O., 2019. Radiance-based retrieval bias mitigation for the MOPITT instrument: The version 8 product. Atmos. Meas. Tech. 12, 4561–4580, Publisher: Copernicus GmbH.

Deeter, M., Francis, G., Gille, J., Mao, D., Martínez-Alonso, S., Worden, H., Ziskin, D., Drummond, J., Commane, R., Diskin, G., McKain, K., 2022. The MOPITT Version 9 CO product: sampling enhancements and validation. Atmos. Meas. Tech. 15 (8), 2325–2344. http://dx.doi.org/10.5194/amt-15-2325-2022, URL: https://amt.copernicus.org/articles/15/2325/2022/.

Deeter, M., Mao, D., Martınez-Alonso, S., Worden, H., Andreae, M., Schlager, H., 2021. Impacts of MOPITT cloud detection revisions on observation frequency and mapping of highly polluted scenes. Remote Sens. Environ. 262, 112516. http://dx.doi.org/10.1016/j.rse.2021.112516, URL: https://www.sciencedirect.com/science/article/pii/S0034425721002364.

Dennison, P.E., Brewer, S.C., Arnold, J.D., Moritz, M.A., 2014. Large wildfire trends in the western United States, 1984–2011. Geophys. Res. Lett. 41, 2928–2933. http://dx.doi.org/10.1002/2014GL059576, publisher: John Wiley & Sons, Ltd.

Dominici, F., Peng, R.D., Barr, C.D., Bell, M.L., 2010. Protecting human health from air pollution: Shifting from a single-pollutant to a multipollutant approach. Epidemiology (Cambridge, Mass.) 21, 187–194. http://dx.doi.org/10.1097/EDE.0b013e3181cc86e8, URL: https://pubmed.ncbi.nlm.nih.gov/20160561.

Drummond, J.R., Zou, J., Nichitiu, F., Kar, J., Deschambaut, R., Hackett, J., 2010. A review of 9-year performance and operation of the MOPITT instrument. Adv. Space Res. 45, 760–774. http://dx.doi.org/10.1016/j.asr.2009.11.019, URL: https://www.sciencedirect.com/science/article/pii/S0273117709007224.

Edwards, D.P., Emmons, L.K., Hauglustaine, D.A., Chu, D.A., Gille, J.C., Kaufman, Y.J., Pétron, G., Yurganov, L.N., Giglio, L., Deeter, M.N., Yudin, V., Ziskin, D.C., Warner, J., Lamarque, J.F., Francis, G.L., Ho, S.P., Mao, D., Chen, J., Grechko, E.I., Drummond, J.R., 2004. Observations of carbon monoxide and aerosols from the Terra satellite: Northern hemisphere variability. J. Geophys. Res.: Atmos. 109, http://dx.doi.org/10.1029/2004JD004727, publisher: John Wiley & Sons, Ltd.

Emmons, L.K., Schwantes, R.H., Orlando, J.J., Tyndall, G., Kinnison, D., Lamarque, J.F., Marsh, D., Mills, M.J., Tilmes, S., Bardeen, C., Buchholz, R.R., Conley, A., Gettelman, A., Garcia, R., Simpson, I., Blake, D.R., Meinardi, S., Pétron, G., 2020. The chemistry mechanism in the community earth system model version

2 (CESM2). J. Adv. Modelling Earth Syst. 12, 000000000. http://dx.doi.org/10.1029/2019MS001882, publisher: John Wiley & Sons, Ltd.

Finlay, S.E., Moffat, A., Gazzard, R., Baker, D., Murray, V., 2012. Health impacts of wildfires. PLoS Curr. 4, e4f959951cce2c. http://dx.doi.org/10.1371/4f959951cce2.c, URL: https://pubmed.ncbi.nlm.nih.gov/23145351, publisher: Public Library of Science.

Ford, B., Va. Martin, M., Zelasky, S.E., Fischer, E.V., Anenberg, S.C., Heald, C.L., Pierce, J.R., 2018. Future fire impacts on smoke concentrations, visibility, and health in the contiguous United States. GeoHealth 2, 229–247. http://dx.doi.org/10.1029/2018GH000144, publisher: John Wiley & Sons, Ltd.

Gaubert, B., Emmons, L.K., Raeder, K., Tilmes, S., Miyazaki, K., Arellan. Jr., A.F, Elguindi, N., Granier, C., Tang, W., Barré, J., Worden, H.M., Buchholz, R.R., Edwards, D.P., Franke, P., Anderson, J.L., Saunois, M., Schroeder, J., Woo, J.H., Simpson, I.J., Blake, D.R., Meinardi, S., Wennberg, P.O., Crounse, J., Teng, A., Kim, M., Dickerson, R.R., He, H., Ren, X., Pusede, S.E., Diskin, G.S., 2020. Correcting model biases of CO in East Asia: Impact on oxidant distributions during KORUS-AQ. Atmos. Chem. Phys 20, 14617–14647. http://dx.doi.org/10.5194/acp-20-14617-2020, URL: https://acp.copernicus.org/articles/20/14617/2020/, publisher: Copernicus Publications.

Gaubert, B., Worden, H.M., Arellano, A.F.J., Emmons, L.K., Tilmes, S., Barré, J., Martine. Alonso, S., Vitt, F., Anderson, J.L., Alkemade, F., Houweling, S., Edwards, D.P., 2017. Chemical feedback from decreasing carbon monoxide emissions. Geophys. Res. Lett. 44, 9985–9995. http://dx.doi.org/10.1002/2017GL074987, publisher: John Wiley & Sons, Ltd.

Granier, C., Darras, S., van der Gon, H.D., Jana, D., Elguindi, N., Bo, G., Michael, G., Marc, G., Jalkanen, J.P., Kuenen, J., 2019. The Copernicus Atmosphere Monitoring Service Global and Regional Emissions (April 2019 Version). Copernicus Atmosphere Monitoring Service.

Guan, H., Chatfield, R.B., Freitas, S.R., Bergstrom, R.W., Longo, K.M., 2008. Modeling the effect of plume-rise on the transport of carbon monoxide over frica with NCAR CAM. Atmos. Chem. Phys. 8, 6801–6812. http://dx.doi.org/10.5194/acp-8-6801-2008, URL: https://acp.copernicus.org/articles/8/6801/2008/.

Guenther, A.B., Jiang, X., Heald, C.L., Sakulyanontvittaya, T., Duhl, T., Emmons, L.K., Wang, X., 2012. The model of emissions of gases and aerosols from nature version 2.1 (MEGAN2.1): An extended and updated framework for modeling biogenic emissions. Geosci. Model Dev 5, 1471–1492. http://dx.doi.org/10.5194/gmd-5-1471-2012, URL: https://gmd.copernicus.org/articles/5/1471/2012/ publisher: Copernicus Publications.

Hedelius, J.K., He, T.L., Jones, D.B.A., Baier, B.C., Buchholz, R.R., D. Maziére, M., Deutscher, N.M., Dubey, M.K., Feist, D.G., Griffith, D.W.T., Hase, F., Iraci, L.T., Jeseck, P., Kiel, M., Kivi, R., Liu, C., Morino, I., Notholt, J., Oh, Y.S., Ohyama, H., Pollard, D.F., Rettinger, M., Roche, S., Roehl, C.M., Schneider, M., Shiomi, K., Strong, K., Sussmann, R., Sweeney, C., Té, Y., Uchino, O., Velazco, V.A., Wang, W., Warneke, T., Wennberg, P.O., Worden, H.M., Wunch, D., 2019. Evaluation of MOPITT Version 7 joint TIR-NIR XCO retrievals with TCCON. Atmos. Meas. Tech. 12, 5547–5572. http://dx.doi.org/10.5194/amt-12-5547-2019, URL: https://amt.copernicus.org/articles/12/5547/2019/, publisher: Copernicus Publications.

Hung, W.T., Lu, C.H.S., Alessandrini, S., Kumar, R., Lin, C.A., 2021. The impacts of transported wildfire smoke aerosols on surface air quality in New York State: A multi-year study using machine learning. Atmos. Environ. 259, 118513. http://dx.doi.org/10.1016/j.atmosenv.2021.118513, URL: https://www.sciencedirect.com/science/article/pii/S1352231021003344.

Kang, C.M., Gold, D., Koutrakis, P., 2014. Downwind O3 and PM2.5 speciation during the wildfires in 2002 and 2010. Atmos. Environ. 95, 511–519. http://dx.doi.org/10.1016/j.atmosenv.2014.07.008, URL: https://www.sciencedirect.com/science/article/pii/S1352231014005299.

Koster, R.D., Darmenov, A., Silva, 2015. The Quick Fire Emissions Dataset (QFED): Documentation of Versions 2.1, 2.2 and 2.4. Vol. 38. Technical ReportSeries, on Global Modeling and Data Assimilation.

Lamarque, J.F., Emmons, L.K., Hess, P.G., Kinnison, D.E., Tilmes, S., Vitt, F., Heald, C.L., Holland, E.A., Lauritzen, P.H., Neu, J., Orlando, J.J., Rasch, P.J., Tyndall, G.K., 2012. CAM-chem: Description and evaluation of interactive atmospheric chemistry in the Community Earth System Model. Geosci. Model Dev. 5, 369–411. http://dx.doi.org/10.5194/gmd-5-369-2012, URL: https://gmd.copernicus.org/articles/5/369/2012/, publisher: Copernicus Publications.

Lapina, K., Honrath, R.E., Owen, R.C., Va. Martın, M., Pfister, G., 2006. Evidence of significant large-scale impacts of boreal fires on ozone levels in the midlatitude Northern Hemisphere free troposphere. Geophys. Res. Lett. 33, http://dx.doi.org/10.1029/2006GL025878, publisher: John Wiley & Sons, Ltd.

Li, S., Banerjee, T., 2021. Spatial and temporal pattern of wildfires in California from 2000 to 2019. Sci. Rep. 11 (8779), http://dx.doi.org/10.1038/s41598-021-88131-9.

Liu, T., Mickley, L.J., Marlier, M.E., DeFries, R.S., Khan, M.F., Latif, M.T., Karambelas, A., 2020. Diagnosing spatial biases and uncertainties in global fire emissions inventories: Indonesia as regional case study. Remote Sens. Environ. 237, 111557. http://dx.doi.org/10.1016/j.rse.2019.111557, URL: https://www.sciencedirect.com/science/article/pii/S0034425719305772.

McClure, C.D., Jaffe, D.A., 2018. US particulate matter air quality improves except in wildfire-prone areas. Proc. Natl. Acad. Sci. 115 (7901), http://dx.doi.org/10.1073/pnas.1804353115, URL: http://www.pnas.org/content/115/31/7901.abstract.

National Interagency Coordination Center (NICC), 2020. Wildland Fire Summary and Statistics Annual Report. Technical Report, URL: https://www.predictiveservices.nifc.gov/intelligence/2020_statssumm/2020Stats&Summ.html.

O' Dell, K., Bilsback, K., Ford, B., Martenies, S.E., Magzamen, S., Fischer, E.V., Pierce, J.R., 2021. Estimated mortality and morbidity attributable to smoke plumes in the United States: Not just a Western US problem. GeoHealth 5, e2021GH000457. http://dx.doi.org/10.1029/2021GH000457, publisher: John Wiley & Sons, Ltd.

Ortega, I., Hannigan, J., Buchholz, R., Pfister, G., 2021. Long-term variability and source signature of gases emitted from oil & natural gas and cattle feedlot operations in the Colorado front range. Atmos. Environ. 263, 118663. http://dx.doi.org/10.1016/j.atmosenv.2021.118663, URL: https://www.sciencedirect.com/science/article/pii/S1352231021004854.

Otte, Tanya L., 2008. The impact of nudging in the meteorological model for retrospective air quality simulations. Part II: Evaluating collocated meteorological and air quality observations. J. Appl. Meteorol. Climatol. 47, 1868–1887. http://dx.doi.org/10.1175/2007JAMC1791.1.

Pan, X., Ichoku, C., Chin, M., Bian, H., Darmenov, A., Colarco, P., Ellison, L., Kucsera, T., d. Silva, A., Wang, J., Oda, T., Cui, G., 2020. Six global biomass burning emission datasets: intercomparison and application in one global aerosol model. Atmos. Chem. Phys. 20, 969–994. http://dx.doi.org/10.5194/acp-20-969-2020, URL: https://acp.copernicus.org/articles/20/969/2020/, publisher: Copernicus Publications.

Pfister, G.G., Emmons, L.K., Hess, P.G., Honrath, R., Lamarque, J.F., Va. Martin, M., Owen, R.C., Avery, M.A., Browell, E.V., Holloway, J.S., Nedelec, P., Purvis, R., Ryerson, T.B., Sachse, G.W., Schlager, H., 2006. Ozone production from the 2004 North American boreal fires. J. Geophys. Res.: Atmos. (111), http://dx.doi.org/10.1029/2006JD007695, publisher: John Wiley & Sons, Ltd.

Phuleria, H.C., Fine, P.M., Zhu, Y., Sioutas, C., 2005. Air quality impacts of the October 2003 Southern California wildfires. J. Geophys. Res.: Atmos. (110), http://dx.doi.org/10.1029/2004JD004626, publisher: John Wiley & Sons, Ltd.

Sodemann, H., Pommier, M., Arnold, S.R., Monks, S.A., Stebel, K., Burkhart, J.F., Hair, J.W., Diskin, G.S., Clerbaux, C., Coheur, P.F., Hurtmans, D., Schlager, H., Blechschmidt, A.M., Kristjánsson, J.E., Stohl, A., 2011. Episodes of cross-polar transport in the Arctic troposphere during July 2008 as seen from models, satellite, and aircraft observations. Atmos. Chem. Phys. 11, 3631–3651. http://dx.doi.org/10.5194/acp-11-3631-2011, URL: https://acp.copernicus.org/articles/11/3631/2011/, publisher: Copernicus Publications.

Steelman, T.A., Burke, C.A., 2007. Is wildfire policy in the United States sustainable? J. Forestry 105, 67–72, ISBN: 0022-1201, Publisher: Oxford University Press Bethesda, MD.

Tang, W., Emmons, L.K., Buchholz, R.R., Wiedinmyer, C., Schwantes, R.H., He, C., Kumar, R., Pfister, G.G., Worden, H.M., Hornbrook, R.S., Apel, E.C., Tilmes, S., Gaubert, B., Martinez-Alonso, S.E., Lacey, F., Holmes, C.D., Diskin, G.S., Bourgeois, I., Peischl, J., Ryerson, T.B., Hair, J.W., Weinheimer, A.J., Montzka, D.D., Tyndall, G.S., Campos, T.L., 2022. Effects of fire diurnal variation and plume rise on U.S. air quality during FIREX-AQ and we-can based on the multi-scale infrastructure for chemistry and aerosols (MUSICAv0). J. Geophys. Res.: Atmos. 127, e2022JD036650. http://dx.doi.org/10.1029/2022JD036650, publisher: John Wiley & Sons, Ltd.

Tang, W., Worden, H.M., Deeter, M.N., Edwards, D.P., Emmons, L.K., Martınez-Alonso, S., Gaubert, B., Buchholz, R.R., Diskin, G.S., Dickerson, R.R., Ren, X., He, H., Kondo, Y., 2020. Assessing measurements of pollution in the troposphere (MOPITT) carbon monoxide retrievals over urban versus non-urban regions. Atmos. Meas. Tech. 13, 1337–1356. http://dx.doi.org/10.5194/amt-13-1337-2020, URL: https://amt.copernicus.org/articles/13/1337/2020/, publisher: Copernicus Publications.

Tilmes, S., Hodzic, A., Emmons, L.K., Mills, M.J., Gettelman, A., Kinnison, D.E., Park, M., Lamarque, J.F., Vitt, F., Shrivastava, M., Campuzano-Jost, P., Jimenez, J.L., Liu, X., 2019. Climate forcing and trends of organic aerosols in the community earth system model (CESM2). J. Adv. Modelling Earth Syst. 11, 4323–4351. http://dx.doi.org/10.1029/2019MS001827, publisher: John Wiley & Sons, Ltd.

Voulgarakis, A., Field, R.D., 2015. Fire influences on atmospheric composition, air quality and climate. Curr. Pollut. Rep. 1, 70–81. http://dx.doi.org/10.1007/s40726-015-0007-z.

Wang, B., Kuang, S., Pfister, G.G., Pour-Biazar, A., Buchholz, R.R., Langford, A.O., Newchurch, M.J., 2021. Impact of the 2016 Southeastern US wildfires on the vertical distribution of ozone and aerosol at Huntsville, Alabama. J. Geophys. Res.: Atmos. 126, e2021JD034796. http://dx.doi.org/10.1029/2021JD034796, URL: https://agupubs.onlinelibrary.wiley.com/doi/abs/10.1029/2021JD034796, _eprint: https://agupubs.onlinelibrary.wiley.com/doi/pdf/10.1029/2021JD034796.

Wiedinmyer, C., Akagi, S.K., Yokelson, R.J., Emmons, L.K., Al-Saadi, J.A., Orlando, J.J., Soja, A.J., 2011. The fire INventory from NCAR (FINN): A high resolution global model to estimate the emissions from open burning. Geosci. Model Dev. 4, 625–641. http://dx.doi.org/10.5194/gmd-4-625-2011, URL: https://gmd.copernicus.org/articles/4/625/2011/.

Xu, R., Yu, P., Abramson, M.J., Johnston, F.H., Samet, J.M., Bell, M.L., Haines, A., Ebi, K.L., Li, S., Guo, Y., 2020. Wildfires, global climate change and human health. New England J. Med. 383, 2173–2181. http://dx.doi.org/10.1056/NEJMsr2028985, URL: https://www.nejm.org/doi/full/10.1056/NEJMsr2028985.

Xue, Z., Gupta, P., Christopher, S., 2021. Satellite-based estimation of the impacts of summertime wildfires on $PM_{2.5}$ concentration in the United States. Atmos. Chem. Phys. 21, 11243–11256. http://dx.doi.org/10.5194/acp-21-11243-2021, URL: https://acp.copernicus.org/articles/21/11243/2021/.

Yang, Z., Demoz, B., Delgado, R., Sullivan, J., Tangborn, A., Lee, P., 2022. Influence of the transported Canadian wildfire smoke on the ozone and particle pollution over the Mid-Atlantic United States. Atmos. Environ. 273, 118940. http://dx.doi.org/10.1016/j.atmosenv.2022.118940, URL: https://www.sciencedirect.com/science/article/pii/S135223102200005X.